JATIS Journal of Astronomical Telescopes, Instruments, and Systems

RESEARCH PAPER

High-redshift extragalactic science with the Single Aperture Large Telescope for Universe Studies (SALTUS) space observatory

Justin Spilker[a,*] **Rebecca C. Levy**[b] **Daniel P. Marrone**[b] **Stacey Alberts**[b] **Scott C. Chapman**[c,d,e] **Mark Dickinson**[f] **Eiichi Egami**[b] **Ryan Endsley**[g] **Desika Narayanan**[h] **George Rieke**[b] **Antony A. Stark**[i] **Alexander Tielens**[j,k] **and Christopher K. Walker**[b]

[a]Texas A&M University, George P. and Cynthia Woods Mitchell Institute for Fundamental Physics and Astronomy, Department of Physics and Astronomy, College Station, Texas, United States
[b]University of Arizona, Department of Astronomy and Steward Observatory, Tucson, Arizona, United States
[c]University of British Columbia, Department of Physics and Astronomy, Vancouver, British Columbia, Canada
[d]National Research Council, Herzberg Astronomy and Astrophysics, Victoria, British Columbia, Canada
[e]Dalhousie University, Department of Physics and Atmospheric Science, Halifax, Nova Scotia, Canada
[f]NSF's NOIRLab, Tucson, Arizona, United States
[g]University of Texas at Austin, Department of Astronomy, Austin, Texas, United States
[h]University of Florida, Department of Astronomy, Gainesville, Florida, United States
[i]Harvard-Smithsonian Center for Astrophysics, Cambridge, Massachusetts, United States
[j]Leiden Observatory, Leiden, The Netherlands
[k]University of Maryland, Astronomy Department, College Park, Maryland, United States

ABSTRACT. We present an overview of the high-redshift extragalactic science case for the Single Aperture Large Telescope for Universe Studies (SALTUS) far-infrared (IR) National Aeronautics and Space Administration probe-class mission concept. Enabled by its 14-m primary reflector, SALTUS offers enormous gains in spatial resolution and spectral sensitivity over previous far-IR missions. SALTUS would be a versatile observatory capable of responding to the scientific needs of the extragalactic community in the 2030s and a natural follow-on to the near- and mid-IR capabilities of JWST. The key early-universe science goals for SALTUS focus on understanding the role of galactic feedback processes in regulating galaxy growth across cosmic time and charting the rise of metals and dust from the early universe to the present. We summarize these science cases and the performance metrics most relevant for high-redshift observations.

Keywords: extragalactic science; terahertz spectroscopy; far-infrared; submillimeter; heterodyne resolution; mission concept

Paper 24052SS received Apr. 25, 2024; revised Jun. 24, 2024; accepted Jul. 15, 2024; published Aug. 20, 2024.

1 Introduction

The Single Aperture Large Telescope for Universe Studies (SALTUS) observatory is a far-infrared (IR) space mission concept proposed to the National Aeronautics and Space Administration under the recent Atacama Pathfinder EXperiment (APEX) call for proposals (Chin et al., subm.). SALTUS would provide $>100\times$ better sensitivity throughout the far-infrared wavelength range ($\approx$30 to 700 μm) compared with past missions, enabled by sensitive

*Address all correspondence to Justin Spilker, jspilker@tamu.edu

2329-4124/2024/$28.00 © 2024 SPIE

instrumentation and a 14-m primary mirror. The large aperture size would also provide $\sim 1''$ spatial resolution at these wavelengths, solving the spatial confusion problems that have plagued past far-IR space observatories. The two instruments planned for SALTUS are High Resolution Receiver (HiRX), a multi-pixel, multi-band heterodyne receiver system (Silva et al., subm.), and SAFARI-Lite, a direct-detection grating spectrometer providing simultaneous 35 to 230 μm spectroscopy (Roelfsema et al., subm.). The overall telescope and spacecraft architectures are described in a series of papers elsewhere in this issue (Arenberg et al., Kim et al., Harding et al. subm.).

The extragalactic science case for SALTUS is centered around the "cosmic ecosystems" theme of the 2020 Decadal Survey in Astronomy and Astrophysics. SALTUS aims to connect measurements of star-forming galaxies and accreting black holes from the nearby universe to high redshifts with the same observables. As the first few years of JWST observations have demonstrated, high angular resolution and sensitive spectroscopy are key to distinguishing galaxies from nearby neighbors and probing the physical conditions of galactic environments, inside and out. With the rapid transition from an initially dust-free universe to its present state in which most star formations and black hole growth are obscured, charting the rise and growth of dust from early times to the present is a key open question. It has also become clear that the feeding of gas into galaxies and the subsequent feedback disrupting the said gas have profound impacts on the short- and long-term growth of galaxies. These high-level questions motivate an observatory capable of sensitive far-IR spectroscopy to detect spectral features associated with these processes without being hampered by the obscuration that plagues shorter wavelengths.

This paper provides an overview of the promise of SALTUS for high-redshift extragalactic science. Accompanying papers describe the plans for guaranteed time and guest observing (Chin et al.), SALTUS's contributions to Milky Way and nearby galaxy science (Levy et al.), star and planet formation (Schwarz et al.), and solar system observations (Anderson et al.). In Sec. 2, we give a high-level overview of the key observable features that enable SALTUS's high-redshift science goals. Section 3 briefly summarizes the most relevant SALTUS performance characteristics for high-redshift observing programs. Section 4 highlights several key high-redshift measurements that would address open questions in the field. We conclude in Sec. 5.

2 Connecting Far-IR Observables to Science Outcomes

The mid- and far-infrared wavelength ranges are unique in the extraordinarily wide range of astrophysical phenomena accessible by atomic and molecular spectral diagnostics. Spectral features trace gas over many orders of magnitude in temperature and density, from cold molecular gas probed by far-IR molecular lines to hot gas traced by high-ionization lines typically associated with black hole accretion. In this section, we provide a brief overview of the various diagnostics keys to SALTUS's high-redshift science case. More detailed descriptions can be found in many previous works, including the study reports for the Space Infrared Telescope for Cosmology and Astrophysics (SPICA) and Origins Space Telescope mission concepts.[1,2] There are many additional features in the rest-frame mid- and far-IR that could be detectable with the sensitivity of SALTUS, including additional fine-structure, crystalline, and ice features, but we focus here on those relevant for our later key science cases.

A key advantage to all of these diagnostics is the near-total insensitivity to dust extinction. With the exception of silicate absorption features at rest-frame 9.7 and 18 μm, dust extinction is negligible throughout the mid- and far-IR, more than an order of magnitude lower than at optical wavelengths (e.g., Refs. 3 and 4). The gas column density N_H likewise does not affect far-IR measurements, in contrast to the strong absorption of X-rays due to hydrogen along the line of sight.

The mid- and far-IR wavelength ranges uniquely allow for simultaneous measurements of both the star formation rate (SFR) and the black hole accretion rate (BHAR) of galaxies through a suite of ionic fine-structure lines (e.g., Refs. 5 and 6). Ions with relatively low ionization potential (e.g., [NeII] 12.8 μm, [NeIII] 15.5 μm, and [SIII] 33.5 μm) are robust tracers of HII regions surrounding young massive stars. More highly ionized species (e.g., [OIV] 25.9 μm, [NeV] 14.3, 24.3 μm) are predominantly produced by the hard ultraviolet (UV) radiation fields surrounding active galactic nuclei (AGNs), providing direct BHAR tracers (e.g., Ref. 7). Cooler ionized and atomic gases in the transition region between massive stars and their parent molecular clouds are

traced by the brightest interstellar medium (ISM) cooling lines, including [CII] 158 μm, [OI] 63 μm, [OIII] 52, 88 μm, and [NII] 122, 205 μm. Because of their connection to the HII regions, these lines have also proved to be useful SFR indicators alone or in combination (e.g., Refs. 8 and 9). Together, these lines provide a complete picture of the interstellar medium of galaxies.

The ratios of these bright spectral lines also allow for robust estimates of the metallicity and abundance patterns in galaxies (e.g., Refs. 10–12). Line ratios of ([NIII] 57 μm) / ([OIII] $52 + 88$ μm), for example, trace the [N/O] abundance pattern,[13] which can either be combined with direct tracers of the H abundance (e.g., free-free emission) or used to estimate galaxy metallicities alone via the correlation between [N/O] and [O/H] (e.g., Refs. 7 and 14). Though studied in far fewer galaxies than the typical strong lines at optical wavelengths, these IR diagnostics will prove especially useful in the dusty galaxies that dominate the total SFR density over the last 12 Gyr of cosmic evolution.[15]

Signatures of galactic feedback processes are also present at IR wavelengths. In spatially unresolved data, massive galactic outflows are typically recognized by the excess flux in the high-velocity wings of spectral lines. Although X-ray diagnostics probe only the very hottest and low-density material in outflows and optical diagnostics provide access to warm ionized gas outflows, the IR is unique in its ability to probe outflowing gas across many orders of magnitude in temperature and density. From the coldest molecular phases that dominate the total outflowing mass (lines of OH, H_2O throughout the far-IR[16,17]) to cool neutral gas ([CII] 158 μm line wings[18]) and to warm ionized gas ([OIII] 52 and 88 μm), a comprehensive census of the gas in galactic winds can uniquely be assembled solely using IR spectroscopy.

At the intersection between few-atom molecules and macroscopic dust grains in the ISM lie polycyclic aromatic hydrocarbons (PAHs), complex organic molecules consisting of hundreds or thousands of atoms. Often thought to represent the small-grain tail of the dust grain size distribution, PAHs have very bright rest-frame mid-IR bands from 3.3 to 17 μm that represent up to 20% of the total IR luminosity[19] and are thus detectable to large distances. Furthermore, the ratios between various PAH features allow for estimates of the grain size distribution, PAH ionization fraction, and ambient radiation field strength.[20]

With PAHs tracing, in effect, the small-size end of the dust grain size distribution, larger grains emit a long-wavelength continuum in accordance with their temperature. Hundreds of thousands of dusty galaxies are known (most without spectroscopic redshift confirmation) due to wide-area surveys with Herschel and ground-based telescopes such as the South Pole Telescope. The broad dust spectral energy distribution (SED), peaking at rest frame $\approx$100 μm, has proved difficult to constrain in the post-Herschel era, resulting in large uncertainties in the total IR luminosity of galaxies based on extrapolations and template fitting. For galaxies with dust-obscured AGN in particular, the relative contribution of cold dust heated predominantly by star formation and warmer dust heated by the AGN is impossible to constrain without rest-frame mid-IR coverage, preventing these two powerful processes from being disentangled. Although imaging surveys with Herschel and ground-based millimeter telescopes often face challenges due to confusion, SALTUS's larger aperture allows the continuum of individual galaxies to be recovered from its wide-band spectrometer (Sec. 3.3). Dust grains can also be probed using the well-known silicate features at 9.7 and 18 μm, which appear prominently in absorption against the bright continuum of AGN.

Finally, the far-IR also provides access to direct and indirect tracers of molecular hydrogen, H_2. The rotational H_2 lines, particularly those at 17.0 and 28.2 μm, are tracers of warm molecular gas ($\sim$200 to 1000 K) in conditions often reached in shocks. Because H_2 itself lacks a permanent dipole moment, it cannot trace colder molecular gas. Its deuterated counterpart HD (56, 112 μm), however, can provide robust estimates of the total molecular gas contents of galaxies because the cosmic deuterium abundance is well known.

3 SALTUS Performance for High-Redshift Science

The design principles of the spacecraft, telescope, and instrumentation for SALTUS are described in a series of papers in this issue (Arenberg et al., Harding et al., Kim et al., and Chin et al.). Far more detailed information can be found in those works, but here, we provide a brief summary of the SALTUS performance metrics as they apply to the common needs of the

high-redshift observational community. Although some spectral lines will be accessible with the heterodyne receiver HiRX at significant lookback times, especially in very IR-luminous sources, most high-redshift science is likely to be carried out using the SAFARI-Lite grating spectrometer instead. We focus here on the SALTUS/SAFARI-Lite performance as relevant for high-redshift science (Roelfsema et al., subm.). SAFARI-Lite is capable of both pointed observations of single interesting objects through deep stare-mode observations and small-scale spectroscopic mapping in an on-the-fly mapping mode. Because the output of SAFARI-Lite mapping observations will be spectroscopic data cubes, continuum "imaging" can also be performed by collapsing along the spectral dimension.

Throughout this section, we compare SALTUS to both past and present IR missions (JWST, Herschel), as well as the now-canceled SPICA mission concept. SPICA was intended to be an European Space Agency (ESA)-led mission consisting of a 2.5-m primary mirror cryogenically cooled to <8 K. We include this comparison to illustrate the contrasts between these two very different mission architectures: SPICA, with a small but very cold primary mirror, and SALTUS, with a much larger primary reflector passively cooled to <40 K.

3.1 Wavelength Coverage

The SAFARI-Lite instrument will provide simultaneous coverage from 34 to 230 μm at a spectral resolution of $R \approx 300$ ($\Delta v \approx 1000$ km s^{-1}). Four co-aligned bands from each of the six spatial pixels are dispersed onto 180-detector microwave kinetic inductance detector (MKID) arrays. This wavelength regime covers the entire rest-frame far-infrared at $z = 0$. During the continued operations of JWST/Mid-InfraRed Instrument (MIRI) and supplemented at longer wavelengths by Atacama large millimeter/submillimeter array (ALMA), these instruments combined will provide nearly uninterrupted access to the entire infrared/submillimeter/millimeter wavelength range.

At higher redshifts, varying bright far-IR fine structure lines redshift into and out of the SAFARI-Lite bandpass (Figs. 4 and 5). Notably, [CII] 158 μm is accessible to $z < 0.45$, [OI] 63 μm to $z < 2.6$, [OI] 145 μm to $z < 0.6$, [OIII] 88 μm to $z < 1.6$, [OIII] 52 μm to $z < 3.4$, and [SiII] 34.8 μm to $z < 5.6$. Conversely, other bright rest-frame mid-IR features redshift into the bandpass, including [SIII] 33.5 μm for $z > 0.01$ and bright lines of [NeII] 12.8 μm and [NeIII] 15.5 μm for $z \gtrsim 1.3$. High-ionization tracers of the BHAR, including [NeV] 14.3 and 24.3 μm and [OIV] 25.9 μm, are similarly accessible for $z > 0.3$. The brightest of the broad PAH features, at 6.2, 7.7, and 11.2 μm, redshift into the SAFARI-Lite bandpass for $z \gtrsim 2$. Finally, the low-lying H_2 rotational transitions at 28.2 and 17.0 μm redshift into the SAFARI-Lite bandpass beginning at $z = 0.2$. At all redshifts, the $R \approx 300$ spectral resolution is sufficient to distinguish closely spaced lines. The most well-known blends are [NeII] 12.8/PAH 12.7 and [OIV] 25.9/[FeII] 26. These features were successfully decomposed even in $R \sim 100$ Spitzer/InfraRed Specrograph (IRS) spectra (e.g., Ref. 21), though the success of this deblending depends on the equivalent widths of both features.

For high-redshift science, the broad and simultaneous wavelength coverage provided by SAFARI-Lite would allow the same spectral diagnostics to be used over a very wide range in wavelength, reducing systematic uncertainties inherent to comparing disparate diagnostics. By filling the gap between JWST/MIRI and ALMA, SALTUS would enable comprehensive and uniform analysis of large galaxy samples across cosmic time using the same observables.

3.2 Point Source Sensitivity

Due to its large 14-m aperture, SAFARI-Lite on SALTUS would offer transformational gains in sensitivity over past far-IR missions. The most directly comparable past instrument was the Photodetector Array Camera and Spectrometer (PACS) on the Herschel Space Observatory. PACS provided $R \sim 1000$ to 3000 integral field spectroscopy over a relatively narrow far-IR bandwidth (≈800 to 3000 km s^{-1}) and could reach typical 5σ, 1-h line sensitivity $\approx 5 \times 10^{-18}$ W m^{-2}. By contrast, SALTUS/SAFARI-Lite reaches 5σ, 1-h line sensitivity limits $< 5 \times 10^{-20}$ W m^{-2} over the full 34 to 230 μm wavelength range simultaneously, improving to $3 - 5 \times 10^{-21}$ W m^{-2} at the short-wavelength end of the bandpass.

In Fig. 1, we compare the point source sensitivity of SALTUS/SAFARI-Lite with other similar instruments, including Spitzer/IRS (low-resolution grating modes), JWST/MIRI MRS, and Herschel/PACS. We also include the far-IR grating spectrometer instrument planned for the now-canceled SPICA mission concept SAFARI (SALTUS/SAFARI-Lite is a scaled-back version of

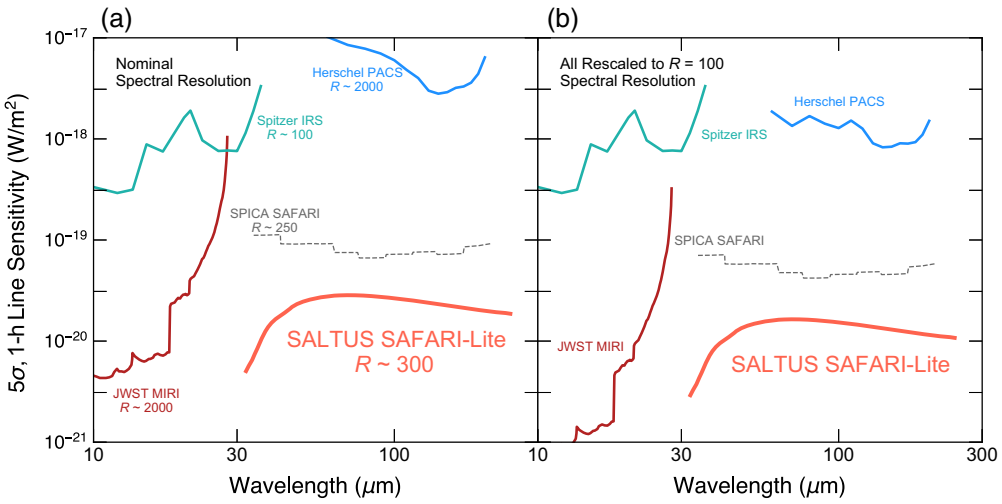

Fig. 1 Comparison of the point source line sensitivities for SALTUS/SAFARI-Lite with other past and existing missions. Panel (a) shows the instrument sensitivities at their nominal spectral resolution, whereas panel (b) rescales all sensitivity curves to a common $R = 100$ spectral resolution to facilitate direct comparisons. This spectral resolution is appropriate for broad features such as redshifted PAH bands. Due to its large 14-m aperture, SALTUS would provide extremely sensitive spectroscopy throughout the far-IR, reaching 2 dex deeper than Herschel and ≈0.5 dex deeper than even the cryogenic 2.5-m SPICA mission concept.

SPICA/SAFARI that removes certain observing modes). This comparison is somewhat complicated by the varying spectral resolution of each instrument. For broad spectral features such as PAH emission, the sensitivity improves to a lower spectral resolution as $R^{1/2}$ (because additional line flux is forced into fewer spectral channels), whereas for narrow lines, it worsens (because wider channels average in additional zero-flux wavelengths and are poorly matched to intrinsically narrow features).

Figure 1 makes it clear that SALTUS/SAFARI-Lite would offer an enormous >100× gain in spectral sensitivity over Herschel/PACS, similar to the gains seen from Spitzer to JWST in the mid-IR. Interestingly, the instrument would also provide substantially better point source sensitivity than SPICA despite the fact that SPICA was planned to have a 2.5-m primary mirror cryogenically cooled to <8 K, in comparison with SALTUS's passively cooled <40 K reflector. The difference arises from the much larger collecting area of SALTUS compared with this smaller, colder mission and continued improvements in far-IR detector performance in the years since the SPICA study concluded. In other words, the 30× larger SALTUS collecting area and improved detectors more than compensate for the additional thermal background emission from the warmer aperture.

3.3 Angular Resolution and (Lack of) Confusion Limits

SALTUS is expected to reach a diffraction-limited angular resolution over its entire wavelength coverage. As a result, SALTUS will offer large gains in resolution compared with Herschel (16× smaller beam area) or smaller ∼2 m mission concepts (more than 50× smaller beam area), reaching ≈1″ resolution throughout the far-IR. This will allow nearby galaxies to be spectroscopically mapped in fine detail, roughly matching the resolution of JWST at mid-IR wavelengths and compact ALMA configurations at long wavelengths. The resolution of SALTUS is illustrated in Fig. 2.

In general, even 1″ resolution will not significantly resolve high-redshift extragalactic targets, which are typically far more compact than local galaxies. The key gain for high-redshift science that SALTUS's high resolution provides is the complete lack of source confusion (see also Chin et al., subm.). Confusion, caused by the collective emission from many unresolved galaxies within a single telescope beam, has long plagued far-IR observatories, including Herschel. Confusion sets a fundamental limit to the faintest object that can be detected in a blind

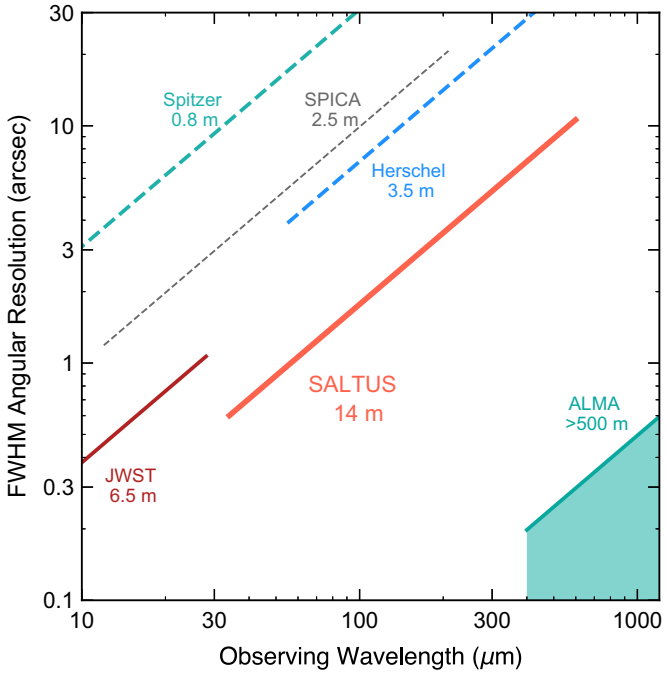

Fig. 2 SALTUS is expected to reach diffraction-limited performance over its entire wavelength range, enabling ≈1″ angular resolution in the far-IR. This would be a substantial improvement over existing or other possible facilities, approximately matching the resolution achievable with JWST at shorter wavelengths and ALMA at longer wavelengths.

survey (e.g., Ref. 22). Reaching beyond this limit requires knowing properties of faint sources *a priori* (e.g., positions and redshifts) to deblend the confused emission.

Confusion was especially problematic for Herschel at long wavelengths because the telescope spatial resolution was poor (36″ at 500 μm) and only 2D imaging data were available. This limit led to the development of deblending techniques that cross-matched with known galaxies from multi-wavelength catalogs (e.g., XID/XID+[23–25]).

Confusion noise also limits far-IR spectrometers for small aperture sizes, even with redshift information as a third dimension to help deblend the confused signal. The flagship-class (≈$10B) Origins Space Telescope mission concept, for example, found that spectral confusion limited the planned science goals for apertures <3.0 m (Ref. 2, Appendix E.1). Even with its planned 5.9-m aperture, only 40% to 70% of sources were recovered by different attempts at extraction from a known input catalog. Worse still, line fluxes—the key observable driving the mission—were poorly recovered, with flux errors approaching a full order of magnitude in some cases.

The problem of confusion is likely to be just as challenging for smaller apertures, but a detailed assessment as a function of aperture size is required. On the one hand, a small aperture has a much larger beam area (scaling as D^{-2}), so even more objects will fall within a single telescope beam. On the other hand, a smaller aperture is less sensitive (instrumental noise also scaling with the collecting area D^{-2}), so perhaps faint confused emission would not have driven the mission design and goals in the first place. The confusion limit and impact on science outcomes is determined by the shape of the galaxy number counts and line luminosity functions as a function of redshift.

Smaller apertures require that the position and redshift of every galaxy in the field be known in advance, which has two main consequences: (1) the continuum emission of galaxies within the beam cannot be recovered reliably without severe assumptions and (2) genuine discovery space is closed off because deblending can only be performed for previously identified galaxies.

The <3″ spatial resolution provided by SALTUS completely eliminates source confusion due to the ≈16× smaller beam area compared with Herschel or ≈50× smaller beam area compared with a 2-m class telescope. Aside from providing surveys with a spatial resolution roughly

matched to those currently being conducted with JWST/MIRI, SALTUS will provide the first confusion-free extragalactic surveys in the far-IR.

3.4 Spectral Survey Speed

The large primary mirror of SALTUS leads to both high sensitivity and high spatial resolution, well-matched to the modest-area surveys currently being conducted with JWST. Slewing and settling the large aperture, however, mean that wide-area surveys are less feasible. SALTUS is capable of mapping an area of $\approx$5 arcmin^2 without repointing using a fine steering mirror. This field of view is very similar to the map sizes produced by single JWST/Near-InfraRed Camera (NIRCam) or MIRI imaging pointings. In terms of resolution, sensitivity, and survey capabilities, SALTUS can be thought of as the far-IR analog of JWST, building on that mission's early success.

The spectral mapping survey speed of SALTUS is comparable to that achievable with smaller 2-m-class apertures, largely because of the substantially better sensitivity of SALTUS. In comparison with surveys with SPICA/SAFARI, for example, SALTUS/SAFARI-Lite could survey a 1-arcmin^2 area to the same depth in an equal amount of observing time but with 30$\times$ more spatial resolution elements.[1] These capabilities lend themselves particularly well to making the first deep far-IR spectral surveys of extragalactic legacy fields over a range in sky area (HUDF, NGDEEP, JADES, GOODS-N, GOODS-S, etc.). Even though SALTUS is not designed for survey-mode operations, its capabilities lend themselves well to JWST-like survey areas and speeds.

4 Key High-Redshift Science Goals for SALTUS

The high-redshift extragalactic science goals of SALTUS are designed to respond to the decadal survey's "cosmic ecosystems" theme and address the key science questions identified for a far-IR probe-class mission. The high-redshift science goals are also highly complementary to observations planned for the nearby universe (see Levy et al., subm.), which will provide a highly resolved anchor for the more distant measurements that we described. As a versatile, extremely sensitive observatory with arcsecond-level spatial resolution, SALTUS would be complementary to the near- and mid-IR capabilities of JWST. In this section, we highlight an ambitious science campaign designed to answer outstanding questions raised by the decadal survey, including How do gas, metals, and dust flow into, through, and out of galaxies? and How do supermassive black holes form and how is their growth coupled with the growth of their host galaxies?

Due to the broad simultaneous wavelength coverage of the SAFARI-Lite instrument in particular, extragalactic observations of individual targets, pointed surveys of well-defined samples, and blank-field spectral mapping campaigns are all capable of addressing different aspects of the cosmic ecosystems science goals. Many of these goals (and beyond) will also be addressed by the wide variety of community guest observer (GO) observing programs enabled by the versatile and sensitive SALTUS capabilities.

4.1 Measure the Rise of Small Dust Grains in the Early Universe

The rapid expansion of our capabilities in the infrared over the last two decades has led to the key discovery that the bulk of active processes in the universe—evolving ISM chemistry and physics, star formation, and black hole accretion—is moderately to heavily obscured by interstellar dust even to high redshifts (e.g., Refs. 26 and 27). This association is more than cosmetic: small-grain cosmic dust plays a key role in the photoelectric heating of gas in the ISM (e.g., Ref. 28) and the formation of molecular hydrogen,[29,30] both of which may give rise to a fundamental relationship between dust and the birth of new stars (e.g., Refs. 31–33).

The rise of cosmic dust in the early universe is therefore a key area of focus in the study of galactic ecosystems. The wealth of diagnostics in a mid-IR galaxy spectrum includes several features arising from small, carbon-rich dust grains termed PAHs, essentially the only spectral features of dust grains accessible at large distances. The strengths and ratios of these features are highly sensitive to their surrounding conditions (i.e., metallicity, radiation field, gas temperature). Advances in the modeling of PAHs (e.g., Refs. 20 and 34) offer the opportunity to constrain the *population* of PAHs to estimate the PAH size distribution and ionization fraction in concert with the radiation field responsible for their heating.

JWST is already providing tantalizing hints at early small grain dust enrichment: recently, the earliest direct detection of a PAH spectral feature at 3.3 μm was made at $z = 4.2$ (~1.5 Gyr after the Big Bang[35]), and a UV feature (the so-called 2175-Å bump) that arises from carbon-rich grains has been observed at $z \gtrsim 7$ (~800 Myr after the Big Bang[36,37]). These observations, combined with the high-redshift (large grain) dust-rich galaxies revealed with ALMA, challenge models of dust production and survival, which limit significant dust build-up to late times (>1.5 Gyr post-Big Bang) via AGB star populations (e.g., Ref. 38). The nature of alternative rapid dust producers will be quantified by JWST at lower redshifts, which has already mapped carbon-rich dust shells around Wolf–Rayet stars[39] and in supernova ejecta[40] at extremely high spatial resolution.

JWST's (and ALMA's) role in directly developing the paradigm of early cosmic dust is limited, however, as neither has the wavelength range to access the rich diagnostic power of the mid-infrared (JWST can only observe one PAH feature at $z \gtrsim 3$). SAFARI-Lite on SALTUS will have the wavelength coverage, spectral resolution, and sensitivity to detect the multiple PAH features in star-forming galaxies at $z \sim 7$ and beyond (Fig. 3).

PAHs play a large role in balancing the heating and cooling processes in the ISM and environments for star formation by catalyzing the formation of H_2 molecules. To extract this information, we need to measure the strengths, equivalent widths, and feature ratios, all of which contain clues to the composition, grain sizes, and ionization states of the molecules (e.g., Refs. 20 and 43–45). Up to $z \approx 5.6$, SAFARI-Lite will simultaneously observe PAH features and the [SiII] 34.8 μm emission line (e.g., Ref. 46). This line is a significant cooling channel in the strong radiation fields expected at high redshift,[47] tracing the cycle of gas heating and cooling in photodissociation regions.

As shown in Fig. 3, SALTUS/SAFARI-Lite is capable of measuring the integrated luminosity of the 6.2, 7.7, 8.6, 11.3, and 12.7 μm PAH features at useful significance even at $z =$ 10 (cosmic age <500 Myr). The expected rapid evolution of interstellar dust in galaxies through

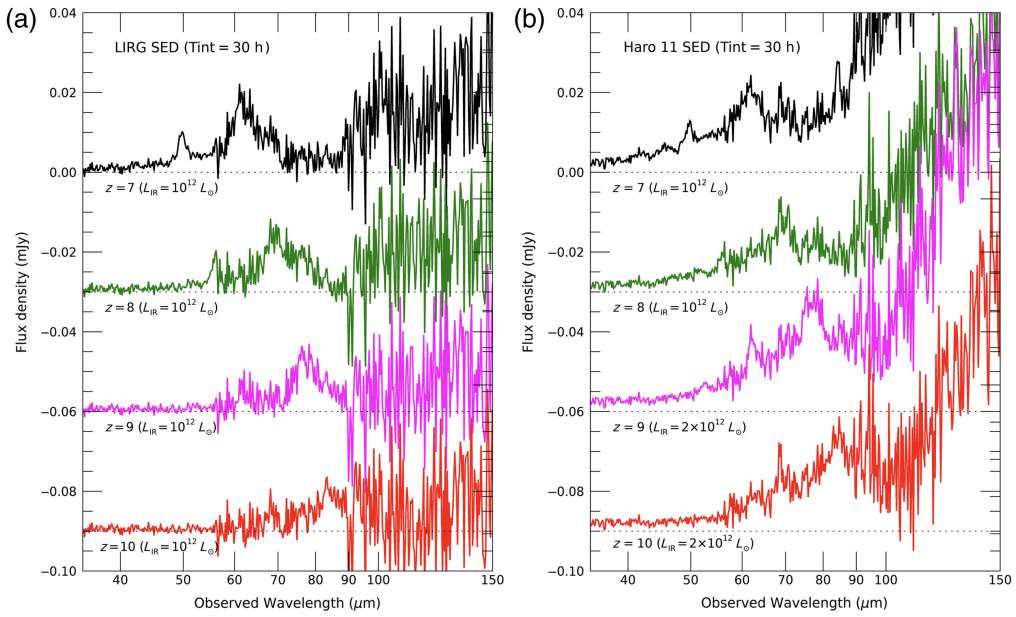

Fig. 3 Simulated SAFARI-Lite PAH spectra for $z \geq 7$ galaxies, for both a dust- and metal-rich LIRG template [the log $L_{IR}/L_{\odot} = 11.75$ template from Ref. 41; (a)] and a lower-metallicity template [Haro 11, 1/3 solar metallicity;[42] (b)]. Low-metallicity dwarf galaxies such as Haro 11 are often considered good analogs of star-forming galaxies at high redshift. As the infrared SEDs of low-metallicity dwarf galaxies are substantially warmer than those of LIRGs, releasing more luminosity in the rest-frame mid-infrared, SAFARI-Lite spectroscopy of high-redshift galaxies is likely to be very effective. We scale each template to the total L_{IR} listed by each curve and simulate a 30-h integration. SALTUS can plausibly detect PAH emission even at $z > 10$. Small carbon grains have already been detected in the UV in this redshift range by JWST,[36,37] and SALTUS will reveal their origin and properties by measuring PAH band ratios. At lower redshifts, all PAH features are easily detected.

the first billion years will be charted through such spectra. In particular, we note that the brightest of the PAH features do not redshift into the noisier long-wavelength channel of SAFARI-Lite until beyond $z > 10$. At lower redshifts $3.5 < z < 7$, SALTUS's sensitivity allows even the faint 17-μm PAH feature to be detected with ease.

4.2 Measure the Co-evolution of Galaxy and Black Hole Growth

The two dominant processes occurring in active, evolving galaxies—the creation of new stars and the accretion of material onto supermassive black holes—are now understood to progress in parallel, with stellar mass and black hole growth rising to a peak during the epoch of cosmic noon before declining to present day.[26] This parallel growth may be fundamental: feedback from black holes ubiquitous in galactic nuclei is widely invoked to regulate the evolution of massive galaxies, a scenario supported by both local observation and theoretical models (e.g., Refs. 48–50). The ubiquity of this pathway, however, is uncertain locally, and both its efficacy and prevalence are even less constrained at higher redshifts (e.g., Refs. 51–53).

Understanding the causal link between star formation and AGNs over cosmic time is a primary goal of the "cosmic ecosystems" SALTUS science theme. The vastly different spatial scales of these processes (kiloparsec versus parsec) have always presented a challenge. The predominant barrier after decades of X-ray and optical studies is that the key phase in any co-evolution is heavily obscured by dust and thus partially or completely invisible to short wavelength observations. Breaking through this barrier requires high-resolution, sensitive far-IR spectroscopy to obtain a direct, unbiased view of the role of AGN in shaping galaxy assembly.

SAFARI-Lite will observe key diagnostics tracing star formation and black hole activity simultaneously in statistical samples of the galaxies that dominate stellar mass growth around cosmic noon ($z \sim 1-4$) and in more luminous galaxies in the early universe ($z > 5$) (Figs. 4 and 5). This is enabled by key far-IR emission lines that have been essentially out of reach for all

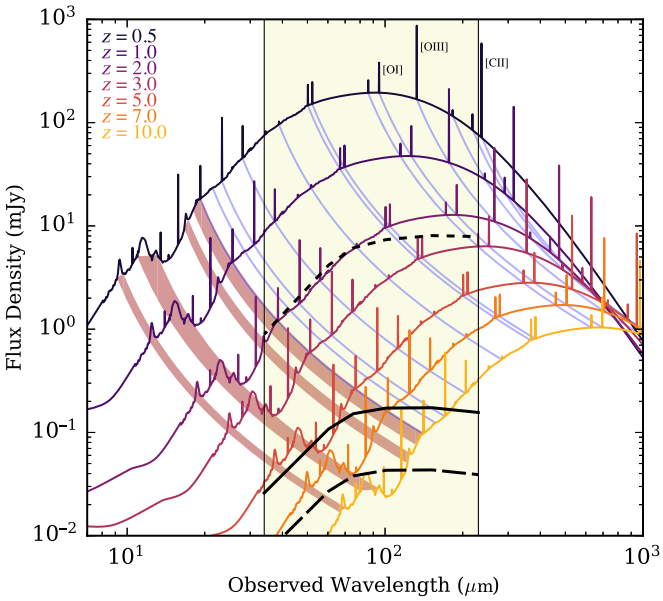

Fig. 4 Spectral range of SALTUS over cosmic time. Schematic representation of the spectral energy distribution of a 3×10^{12} $L_\odot$ star-forming galaxy with redshift using the low-redshift galaxy Haro 11 as a template. Lines important to the science case and PAH features are traced through redshift, and dominant cooling lines ([OI], [OIII], and [CII]) are labeled. Out to $z \sim 3$, SAFARI-Lite probes the peak of the dust continuum and the bulk of the dust emission. Beyond $z \sim 3$, SAFARI-Lite takes over from JWST/MIRI to probe the red-shifted mid-IR PAH emission features. The yellow color-coded region indicates the wavelength range of SAFARI-Lite. The lower solid black curve is the detection limit for SAFARI-Lite at $R = 300$ for pointed observations (1 h, 5σ). The lower long-dashed line approximates a detection limit for wide PAH features, which span many channels. The short-dashed line is the SAFARI-Lite detection limit in mapping mode (1 arcmin^2 area mapped in 1-h at 5σ).

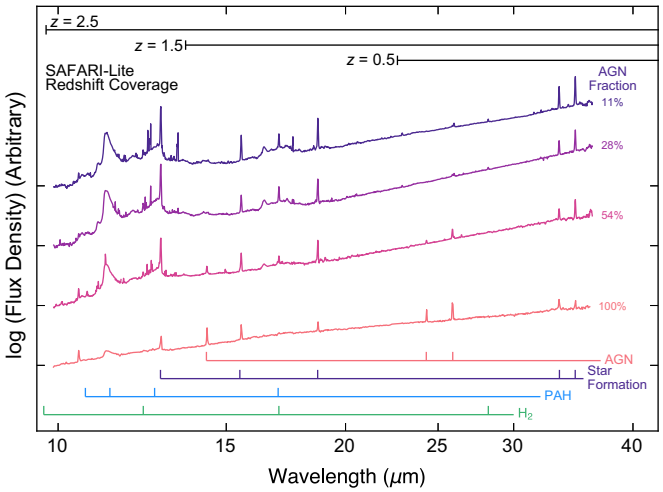

Fig. 5 The rest-frame mid-IR is rich with diagnostics of star formation, AGN, galactic feedback/outflows, and shocks/warm H_2. For $z > 0.5$ and extending beyond the peak of cosmic star formation, SAFARI-Lite will detect or constrain features probing each of these components in thousands of individual galaxies. Colored curves show template spectra for stacks of galaxies observed by Spitzer, ordered by the strength of the AGN contribution to the total luminosity.[54]

previous far-IR missions due to insufficient sensitivity or limited wavelength coverage, complementing JWST and ALMA at shorter and longer wavelengths. The fine structure lines [OIII] 88 μm and [CII] 158 μm will provide star formation rates to $z \sim 1.6$, whereas the rest-frame mid-IR [NeII] 12.8 μm and [NeIII] 15.5 μm are accessible from $z = 1.6$ to beyond $z > 10$. The high-excitation [NeV] 14 and 24 μm, [NeVI] 7.6 μm, and [OIV] 26 μm lines serve similar roles for black hole accretion rates (e.g., Refs. 54 and 55).

This analysis made possible by SALTUS is the only pathway to link star formation and AGN during the dust-obscured phase and establish the timing and thus relative importance of AGN activity in driving and/or quenching star formation. Simultaneously, SAFARI-Lite observations will provide a highly detailed analysis of the spectral features that reveal the suspected mechanism of this co-evolution: outflows driven by AGN feedback (Sec. 4.3). This comprehensive approach will provide the breakthrough that drives our empirical and theoretical galaxy evolution models.

4.3 Measure Galactic Outflows Across Cosmic Time

One of the most important realizations of the past two decades is the vital role that self-regulating feedback processes play in galaxy evolution. Feedback plays a crucial role in explaining many of the fundamental galaxy scaling relationships, including the quenching of star formation in "red and dead" galaxies; the enrichment of heavy elements to great distances beyond a galaxy's stellar disk; and the connection between dark matter halos, star formation, stars, and supermassive black holes. Due to the large dynamic range of spatial and temporal scales over which it manifests, feedback remains the key unknown for cosmological simulations, resulting in a panoply of pre- and post-dictions for galaxy properties that differ by orders of magnitude.

Tracking the impact of feedback from an observational standpoint is a field in its nascency. Powerful galactic outflows of gas are clear feedback signatures and ubiquitously observed in the local universe, but detecting these outflows across cosmic time remains difficult even in the JWST era. In large part, this is because the gas in outflows spans at least six orders of magnitude in both temperature and density (e.g., Ref. 56), so it is difficult for any single observatory to detect and characterize a large portion of the outflowing material.

The far-IR wavelength regime uniquely offers access to outflow tracers ranging from the cold molecular phase (transitions of H_2O, OH), cool atomic gas ([CII] 158 μm, [SiII] 34.8 μm, and [FeII] 26 μm), and warm ionized gas ([SIII] 33 μm and [OIII] 52 and 88 μm) that fall within the SAFARI-Lite bandpass from the nearby universe to cosmic noon, $z \sim 2$ (Fig. 4). In these spectral features, outflows manifest as high-velocity line wings (in emission or, for the molecular

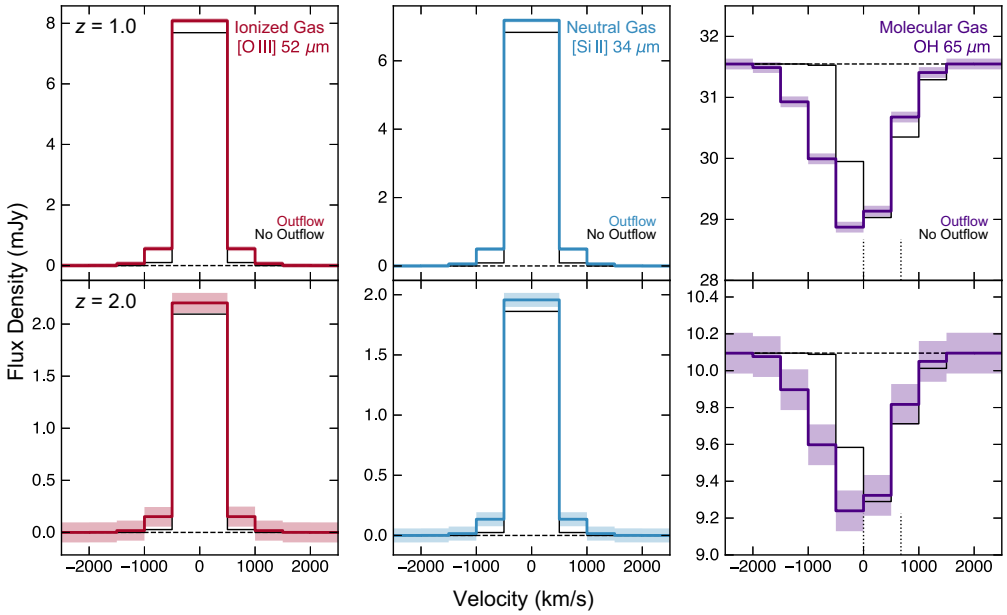

Fig. 6 SALTUS/SAFARI-Lite will inventory galactic outflows with simultaneous observations of the cold molecular, cool atomic, and warm ionized gas phases detected using various far-IR spectral features. We show simulated spectra for a 1-h observation of a $L_{IR} = 2 \times 10^{12}$ $L_\odot$ galaxy with (thick colored lines) or without (thin black lines) a $v_{out} = 700$ km s^{-1} outflow. Colored shaded bands show the 1σ uncertainty per channel. The broad outflow components are detected at both $z = 1$ (top row) and $z = 2$ (bottom row), especially in comparison with the no-outflow spectra.

phase, in absorption against the dust continuum). Although the fastest outflows driven by supernova feedback will also be detectable, SALTUS's science goal in this area is more narrowly focused on AGN-driven winds, which typically reach fast > 1000 km s^{-1} velocities distinguishable at the $R \sim 300$ spectral resolution of SAFARI-Lite (see also similar calculations performed for SPICA/SAFARI at the same spectral resolution[57]).

We illustrate the ability to recover multi-phase outflows using SALTUS/SAFARI-Lite observations in Fig. 6. We created mock spectra at the (Nyquist-sampled) $R = 300$ spectral resolution for a fiducial galaxy with $L_{IR} = 2 \times 10^{12}$ $L_\odot$ at redshifts $z = 1.0, 2.0$, either including or excluding an outflow component to the spectra. For the molecular phase, we simulated the OH 65-μm doublet; for the neutral atomic, [SiII] 34.8 μm; and for the ionized phase, [OIII] 52 μm. We used the IR spectral line scaling relations of Ref. 58 to define the non-outflow line fluxes. We assumed a nominal galaxy intrinsic line width of 400 km s^{-1} and a typical outflow velocity $v_{out} = 700$ km s^{-1}. We assumed an OH absorption depth of $\approx$5% of the continuum, similar to low- and high-redshift studies (e.g., Refs. 17 and 59), and for the emission lines, we assumed a broad-wing amplitude of 10% of the line peak, similar to star-forming galaxies at higher redshifts observed with ALMA.[60] Finally, we assumed a 1-h observation to determine the significance of the outflow component recovery.

Figure 6 demonstrates that SALTUS will easily recover multi-phase outflow components in IR-luminous galaxies to cosmic noon and beyond. Even in a 1-h observation, broad line wings and blueshifted absorption features are detected at very high significance at $z = 1$ (implying that outflows could also be detected in lower-luminosity galaxies) and are recoverable at lower significance at $z = 2$. We note especially that the outflow spectra are distinct from the same spectra that lack an outflow component, i.e., SALTUS can discern the presence versus the absence of outflows. SALTUS enables a comprehensive, multi-phase characterization of AGN-driven outflows that cannot be pieced together using existing or near-future observatories.

This science goal is highly complementary to the objectives outlined in Sec. 4.2. Multi-phase outflow tracers will be covered alongside key diagnostics of the star formation and black hole accretion rates commensally every time the telescope observes an extragalactic target, simultaneously detecting dust-immune metallicity indicators such as [NIII]/[OIII]. Over the mission

lifetime, SALTUS will establish a complete library of galaxy star formation and black hole accretion rates with accompanying measurements of the outflow properties in the hot, cool, and cold gas phases in thousands of individual galaxies.

4.4 Example Community Science in the JWST+SALTUS Era: Obscured AGN at Reionization

Although we have focused primarily on key science goals that helped drive the architecture of the mission, the large majority of SALTUS observations will be carried out by the community through a standard Guest Observer Program (Chin et al. JATIS). Depending on operational efficiency, the SALTUS mission plan calls for 4000 to 5500 h of community observations per year over a minimum 5-year baseline mission duration, comparable to the time currently available on JWST.

One early lesson from JWST's first year is that rapid advances are made possible when large windows in discovery space are opened: unexpected galaxy populations are found for the first time, objects that were once thought to be rare are revealed to be common, and flawed assumptions from previous galaxy models are laid bare. Due to its sensitivity and lack of spatial/spectral confusion, SALTUS will allow a similar new discovery space to be opened, allowing the observatory to be nimble enough to address not only the science questions of the year 2024 but also the unknown questions that will be raised in the 2030s. We illustrate this responsiveness in the face of a recent unexpected JWST finding: that obscured AGN at very high redshifts may be far more common than previously expected.

Within the past year, JWST and ALMA observations have revealed an astonishing number of obscured or heavily reddened AGN at $5 < z < 10$ (e.g., Refs. 61–65). These spectroscopically confirmed AGNs are at least ~30 to 100× more common than previously expected (e.g., Ref. 66) and therefore imply dramatic revisions to our understanding of early supermassive black hole growth. SALTUS is the only observatory capable of delivering much-needed constraints on the bolometric luminosities (and hence black hole growth rates) of these new, reionization-era AGNs, as well as the origin of their dust obscuration.

We expect a single 10-h, 10 arcmin^2 pointing with SALTUS to detect the mid-to-far infrared continua of ~10 to 30 obscured or heavily reddened AGNs at $5 < z < 10$ given recent number density measurements from JWST.[64] These continuum measurements from SALTUS will provide our only direct probe of the warm and hot dust emission from the AGN torus around these very high-redshift AGNs. Even the longest wavelength band with JWST/MIRI (~24 μm) only probes up to rest frame 3 μm at $z = 7$, far bluer than the peak of AGN dust emission (rest ~10 to 30 μm). Given the large diversity in mid-to-far infrared SED shapes of AGN (e.g., Ref. 67), accurate constraints on the bolometric AGN luminosities, and hence the black hole accretion rates, of these systems will only be possible by combining JWST data with measurements from SALTUS. Such data are critical to filling the huge hole in our census of very early black hole accretion density from this new and surprisingly abundant population of $z > 5$ AGN.

Targeted follow-up with SALTUS will yield a ~10σ spectroscopic continuum detection within minutes for the brightest known obscured AGN at $z > 5$. The archetype example is COS-87259, which is confirmed to lie at $z = 6.853$ within the 1.5 deg^2 cosmic evolution survey (COSMOS) field.[61] Several broadband photometric detections with Spitzer/MIPS, Herschel/PACS, and Herschel/Spectral and Photometric Imaging Receiver (SPIRE) indicate that this obscured AGN has a flux density of ~0.3 to 10 mJy that rises between an observed frame of 34 to 230 μm (Fig. 7). The unprecedented mid- and far-infrared sensitivity and spectroscopic capabilities of SALTUS will not only dramatically improve constraints on the bolometric AGN luminosity of this system but also enable the much-needed measurement of the rest-frame 9.7-μm silicate absorption feature in this system. This silicate absorption feature is a highly valuable tracer of the amount of obscuration toward heavily buried AGN such as COS-87259, which cannot be detected in deep X-ray imaging (e.g., Ref. 68). This feature also provides an estimate of the amount of obscuration due to the host galaxy ISM rather than circumnuclear dust, though its origins are still debated (e.g., Ref. 69). Such information is necessary to begin testing recent theoretical models that imply that the higher gas fractions and denser ISM of high-redshift galaxies will more readily lead to heavy AGN obscuration (e.g., Refs. 70 and 71). COS-87259 was found within a relatively small field, and we expect future surveys to rapidly identify many more

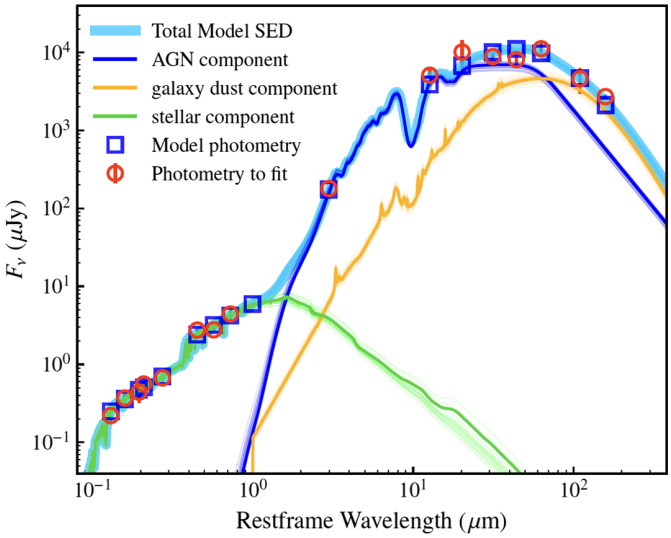

Fig. 7 In its first year of operations, JWST has found an unexpected population of abundant obscured AGN at very high redshifts, including COSMOS-87259 shown here. SALTUS offers the ability to synergize with JWST discoveries into the 2030s due to its large aperture and lack of confusion limit. In this particular example, SALTUS would detect the mid-IR continuum and 9.7-μm silicate feature (if present) in <1 h on-source. Reproduced with permission from Ref. 61.

similar systems (e.g., Ref. 72). These will be excellent targets for pointed follow-up with SALTUS to deliver statistical constraints on the black hole growth rates, as well as the extent and origin of obscuration among the most luminous, buried AGN in the reionization era.

We emphasize that this is only a single example drawn from the first year of JWST operations. Due to the confusion limits that have plagued small apertures in the far-IR, discovery space is limited only to those objects with positions and redshifts that were already known. In addition, detailed measurements to constrain the natures of the sources such as bolometric luminosities and the relative role of star formation are severely compromised by confusion noise. SALTUS mitigates these limitations, enabling the discovery of previously unknown galaxy populations and synergy with other long-wavelength facilities, including JWST.

5 Conclusions

From Sec. 3, it is clear that any future far-IR facility will offer transformative gains over previous observatories at this wavelength. Herschel's defining legacy for the distant universe is its large-area sensitive photometric mapping, but its relatively small aperture resulted in challenging problems from confusion noise that continue to be explored today. Herschel generally lacked the sensitivity for high-redshift spectroscopy, even in large samples of IR-luminous galaxies.[73,74] SALTUS would offer the first chance to probe the wealth of mid- and far-IR spectral diagnostics in galaxies throughout the universe, with no spatial or spectral confusion. Priority high-redshift measurements would detect small dust grains into the reionization epoch to measure the buildup of the dusty universe, simultaneously detect dust-immune indicators of star formation and black hole accretion in galaxies to cosmic noon and beyond, and measure the multi-phase gas in fast galactic outflows that slow future galaxy growth and feed the circumgalactic medium. Its versatile capabilities ensure that SALTUS will also be responsive to the needs of the high-redshift community of the 2030s, after a decade of JWST operations, answering questions that JWST has only just begun to pose.

Disclosures

The authors report no conflicts of interest.

Code and Data Availability

No code or data were used in the preparation of this paper.

References

1. P. R. Roelfsema et al., "SPICA-a large cryogenic infrared space telescope: unveiling the obscured universe," *Publ. Astron. Soc. Aus.* **35**, e030 (2018).
2. M. Meixner et al., "Origins space telescope mission concept study report," arXiv:1912.06213 (2019).
3. J. E. Chiar and A. G. G. M. Tielens, "Pixie dust: the silicate features in the diffuse interstellar medium," *Astrophys. J.* **637**, 774–785 (2006).
4. S. Wang and X. Chen, "The optical to mid-infrared extinction law based on the APOGEE, Gaia DR2, Pan-STARRS1, SDSS, APASS, 2MASS, and WISE Surveys," *Astrophys. J.* **877**, 116 (2019).
5. L. Spinoglio and M. A. Malkan, "Infrared line diagnostics of active galactic nuclei," *Astrophys. J.* **399**, 504 (1992).
6. A. Feltre et al., "Optical and mid-infrared line emission in nearby Seyfert galaxies," *Astron. Astrophys.* **675**, A74 (2023).
7. L. Spinoglio et al., "SOFIA observations of far-ir fine-structure lines in galaxies to measure metallicity," *Astrophys. J.* **926**, 55 (2022).
8. I. De Looze et al., "The applicability of far-infrared fine-structure lines as star formation rate tracers over wide ranges of metallicities and galaxy types," *Astron. Astrophys.* **568**, A62 (2014).
9. S. Mordini, L. Spinoglio, and J. A. Fernández-Ontiveros, "Calibration of mid- to far-infrared spectral lines in galaxies," *Astron. Astrophys.* **653**, A36 (2021).
10. T. Nagao et al., "Metallicity diagnostics with infrared fine-structure lines," *Astron. Astrophys.* **526**, A149 (2011).
11. M. Pereira-Santaella et al., "Far-infrared metallicity diagnostics: application to local ultraluminous infrared galaxies," *Mon. Not. R. Astron. Soc.* **470**, 1218–1232 (2017).
12. D. Rigopoulou et al., "On the far-infrared metallicity diagnostics: applications to high-redshift galaxies," *Mon. Not. R. Astron. Soc.* **473**, 20–29 (2018).
13. B. Peng et al., "Far-infrared line diagnostics: improving N/O abundance estimates for dusty galaxies," *Astrophys. J.* **908**, 166 (2021).
14. Y. Chen et al., "Accurate oxygen abundance of interstellar gas in Mrk 71 from optical and infrared spectra," *Nat. Astron.* **7**, 771–778 (2023).
15. N. Chartab et al., "Low gas-phase metallicities of ultraluminous infrared galaxies are a result of dust obscuration," *Nat. Astron.* **6**, 844–849 (2022).
16. E. González-Alfonso et al., "The Mrk 231 molecular outflow as seen in OH," *Astron. Astrophys.* **561**, A27 (2014).
17. J. S. Spilker et al., "Ubiquitous molecular outflows in $z > 4$ massive, dusty galaxies. I. Sample overview and clumpy structure in molecular outflows on 500 pc scales," *Astrophys. J.* **905**, 85 (2020).
18. R. Herrera-Camus et al., "Kiloparsec view of a typical star-forming galaxy when the Universe was ∼1 Gyr old. I. Properties of outflow, halo, and interstellar medium," *Astron. Astrophys.* **649**, A31 (2021).
19. A. Smercina et al., "After the fall: the dust and gas in E+A post-starburst galaxies," *Astrophys. J.* **855**, 51 (2018).
20. B. T. Draine et al., "Excitation of polycyclic aromatic hydrocarbon emission: dependence on size distribution, ionization, and starlight spectrum and intensity," *Astrophys. J.* **917**, 3 (2021).
21. J. D. T. Smith et al., "The mid-infrared spectrum of star-forming galaxies: global properties of polycyclic aromatic hydrocarbon emission," *Astrophys. J.* **656**, 770–791 (2007).
22. H. Dole et al., "Confusion of extragalactic sources in the mid- and far-infrared: Spitzer and beyond," *Astrophys. J. Supp.* **154**, 93–96 (2004).
23. I. G. Roseboom et al., "The Herschel Multi-Tiered Extragalactic Survey: source extraction and cross-identifications in confusion-dominated SPIRE images," *Mon. Not. R. Astron. Soc.* **409**, 48–65 (2010).
24. P. D. Hurley et al., "HELP: XID+, the probabilistic de-blender for Herschel SPIRE maps," *Mon. Not. R. Astron. Soc.* **464**, 885–896 (2017).
25. D. Liu et al., ""Super-deblended" dust emission in galaxies. I. The GOODS-north catalog and the cosmic star formation rate density out to redshift 6," *Astrophys. J.* **853**, 172 (2018).
26. P. Madau and M. Dickinson, "Cosmic star-formation history," *Ann. Rev. Astron. Astrophys.* **52**, 415–486 (2014).
27. J. A. Zavala et al., "The evolution of the IR luminosity function and dust-obscured star formation over the past 13 billion years," *Astrophys. J.* **909**, 165 (2021).
28. A. G. G. M. Tielens and D. Hollenbach, "Photodissociation regions. I. Basic model," *Astrophys. J.* **291**, 722–746 (1985).

29. J. Bauschlicher and W. Charles, "The reaction of polycyclic aromatic hydrocarbon cations with hydrogen atoms: the astrophysical implications," *Astrophys. J. Lett.* **509**, L125–L127 (1998).
30. N. Foley et al., "Molecular hydrogen formation on interstellar PAHs through Eley-Rideal abstraction reactions," *Mon. Not. R. Astron. Soc.* **479**, 649–656 (2018).
31. M. W. Regan et al., "The radial distribution of the interstellar medium in disk galaxies: evidence for secular evolution," *Astrophys. J.* **652**, 1112–1121 (2006).
32. A. Pope et al., "Probing the interstellar medium of $z \sim 1$ ultraluminous infrared galaxies through interferometric observations of CO and spitzer mid-infrared spectroscopy," *Astrophys. J.* **772**, 92 (2013).
33. I. Cortzen et al., "PAHs as tracers of the molecular gas in star-forming galaxies," *Mon. Not. R. Astron. Soc.* **482**, 1618–1633 (2019).
34. D. Rigopoulou et al., "The properties of polycyclic aromatic hydrocarbons in galaxies: constraints on PAH sizes, charge and radiation fields," *Mon. Not. R. Astron. Soc.* **504**, 5287–5300 (2021).
35. J. S. Spilker et al., "Spatial variations in aromatic hydrocarbon emission in a dust-rich galaxy," *Nature* **618**, 708–711 (2023).
36. J. Witstok et al., "Carbonaceous dust grains seen in the first billion years of cosmic time," *Nature* **621**, 267–270 (2023).
37. V. Markov et al., "Dust attenuation evolution in $z \sim 2-12$ JWST galaxies," arXiv:2402.05996 (2024).
38. M. J. Michałowski, "Dust production 680-850 million years after the Big Bang," *Astron. Astrophys.* **577**, A80 (2015).
39. R. M. Lau et al., "Nested dust shells around the Wolf-Rayet binary WR 140 observed with JWST," *Nat. Astron.* **6**, 1308–1316 (2022).
40. M. Shahbandeh et al., "JWST NIRSpec+MIRI observations of the nearby type IIP supernova 2022acko," arXiv:2401.14474 (2024).
41. G. H. Rieke et al., "Determining star formation rates for infrared galaxies," *Astrophys. J.* **692**, 556–573 (2009).
42. J. Lyu, G. H. Rieke, and S. Alberts, "The contribution of host galaxies to the infrared energy output of $z \gtrsim 5.0$ quasars," *Astrophys. J.* **816**, 85 (2016).
43. A. Li and B. T. Draine, "Infrared emission from interstellar dust. II. The diffuse interstellar medium," *Astrophys. J.* **554**, 778–802 (2001).
44. A. Maragkoudakis, E. Peeters, and A. Ricca, "Probing the size and charge of polycyclic aromatic hydrocarbons," *Mon. Not. R. Astron. Soc.* **494**, 642–664 (2020).
45. O. V. Egorov et al., "PHANGS-JWST first results: destruction of the PAH molecules in H II regions probed by JWST and MUSE," *Astrophys. J. Lett.* **944**, L16 (2023).
46. J. McKinney et al., "Regulating star formation in nearby dusty galaxies: low photoelectric efficiencies in the most compact systems," *Astrophys. J.* **908**, 238 (2021).
47. M. J. Kaufman, M. G. Wolfire, and D. J. Hollenbach, "[Si II], [Fe II], [C II], and H_2 emission from massive star-forming regions," *Astrophys. J.* **644**, 283–299 (2006).
48. P. F. Hopkins et al., "A cosmological framework for the co-evolution of quasars, supermassive black holes, and elliptical galaxies. I. Galaxy mergers and quasar activity," *Astrophys. J. Supp.* **175**, 356–389 (2008).
49. D. Ceverino et al., "Early formation of massive, compact, spheroidal galaxies with classical profiles by violent disc instability or mergers," *Mon. Not. R. Astron. Soc.* **447**, 3291–3310 (2015).
50. S. Veilleux et al., "Cool outflows in galaxies and their implications," *Astron. Astrophys. Rev.* **28**, 2 (2020).
51. J. Runburg et al., "Consistent analysis of the AGN LF in X-ray and MIR in the XMM-LSS field," *Astrophys. J.* **924**, 133 (2022).
52. F. Pacucci et al., "JWST CEERS and JADES active galaxies at z = 4-7 violate the local M.-M_* relation at $>3\sigma$ implications for low-mass black holes and seeding models," *Astrophys. J. Letters* **957**, L3 (2023).
53. M. A. Stone et al., "Undermassive host galaxies of five $z \sim 6$ luminous quasars detected with JWST," *Astrophys. J.* **964**, 90 (2024).
54. M. Stone et al., "Measuring star formation and black hole accretion rates in tandem using mid-infrared spectra of local infrared luminous galaxies," *Astrophys. J.* **934**, 27 (2022).
55. A. Sajina, M. Lacy, and A. Pope, "The past and future of mid-infrared studies of AGN," *Universe* **8**, 356 (2022).
56. E. E. Schneider and B. E. Robertson, "Hydrodynamical coupling of mass and momentum in multiphase galactic winds," *Astrophys. J.* **834**, 144 (2017).
57. E. González-Alfonso et al., "Feedback and feeding in the context of galaxy evolution with SPICA: direct characterisation of molecular outflows and inflows," *Publ. Astron. Soc. Aus.* **34**, e054 (2017).
58. L. Spinoglio et al., "Far-IR/submillimeter spectroscopic cosmological surveys: predictions of infrared line luminosity functions for z < 4 galaxies," *Astrophys. J.* **745**, 171 (2012).
59. E. González-Alfonso et al., "Molecular outflows in local ULIRGs: energetics from multitransition OH analysis," *Astrophys. J.* **836**, 11 (2017).

60. H. B. Akins et al., "ALMA reveals extended cool gas and hot ionized outflows in a typical star-forming galaxy at Z = 7.13," *Astrophys. J.* **934**, 64 (2022).
61. R. Endsley et al., "ALMA confirmation of an obscured hyperluminous radio-loud AGN at z = 6.853 associated with a dusty starburst in the 1.5 deg^2 COSMOS field," *Mon. Not. R. Astron. Soc.* **520**, 4609–4620 (2023).
62. L. J. Furtak et al., "JWST UNCOVER: extremely red and compact object at $z_{\rm phot} \simeq 7.6$ triply imaged by A2744," *Astrophys. J.* **952**, 142 (2023).
63. A. D. Goulding et al., "UNCOVER: the growth of the first massive black holes from JWST/NIRSpec—spectroscopic redshift confirmation of an X-ray luminous AGN at z = 10.1," *Astrophys. J. Lett.* **955**, L24 (2023).
64. J. E. Greene et al., "UNCOVER spectroscopy confirms a surprising ubiquity of AGN in red galaxies at $z > 5$," https://ui.adsabs.harvard.edu/abs/2024ApJ...964...39G/abstract (2023).
65. V. Kokorev et al., "UNCOVER: a NIRSpec identification of a broad-line AGN at $z = 8.50$," *Astrophys. J. Lett.* **957**, L7 (2023).
66. X. Shen et al., "The bolometric quasar luminosity function at z = 0-7," *Mon. Not. R. Astron. Soc.* **495**, 3252–3275 (2020).
67. J. Lyu, G. H. Rieke, and Y. Shi, "Dust-deficient palomar-green quasars and the diversity of AGN intrinsic IR emission," *Astrophys. J.* **835**, 257 (2017).
68. R. C. Hickox and D. M. Alexander, "Obscured active galactic nuclei," *Ann. Rev. Astron. Astrophys.* **56**, 625–671 (2018).
69. D. Farrah et al., "Far-infrared fine-structure line diagnostics of ultraluminous infrared galaxies," *Astrophys. J.* **776**, 38 (2013).
70. M. Trebitsch et al., "Escape of ionizing radiation from high-redshift dwarf galaxies: role of AGN feedback," *Mon. Not. R. Astron. Soc.* **478**, 5607–5625 (2018).
71. Y. Ni et al., "QSO obscuration at high redshift ($z \gtrsim 7$): predictions from the bluetides simulation," *Mon. Not. R. Astron. Soc.* **495**, 2135–2151 (2020).
72. J. Lyu et al., "AGN selection and demographics: a new age with JWST/MIRI," https://ui.adsabs.harvard.edu/abs/2024ApJ...966..229L/abstract (2023).
73. J. L. Wardlow et al., "The interstellar medium in high-redshift submillimeter galaxies as probed by infrared spectroscopy*," *Astrophys. J.* **837**, 12 (2017).
74. D. Wilson et al., "Stacked average far-infrared spectrum of dusty star-forming galaxies from the Herschel/SPIRE Fourier transform spectrometer," *Astrophys. J.* **848**, 30 (2017).

Justin Spilker is an assistant professor in the Department of Physics and Astronomy and the Mitchell Institute of Texas A&M University.

Rebecca C. Levy is an NSF Astronomy and Astrophysics Postdoctoral Fellow at the University of Arizona.

Daniel P. Marrone is a professor of astronomy at the University of Arizona.

Stacey Alberts is an assistant professor at the University of Arizona.

Mark Dickinson is an astronomer at NSF's National Optical-Infrared Astronomy Research Laboratory.

Eiichi Egami is a research professor at the University of Arizona.

George Rieke is a Regents' professor of astronomy and planetary sciences at the University of Arizona.

Alexander Tielens is a professor of astronomy in the Astronomy Department of the University of Maryland, College Park.

Christopher K. Walker is a professor of astronomy at the University of Arizona and the principal investigator of the SALTUS mission concept.

Biographies of the other authors are not available.